Bifunctional 3D POM-Based Coordination Polymers for Improved Pseudocapacitance and Catalytic Oxidation Performance

Yujiao Hou,* Peilin Han, Hao Li, Shixing Zhang Mengge Qin, Nan Zhang, Bingbing Fu, Ruitao Mao, Suxiang Ge*

College of Chemical and Materials Engineering, Xuchang University, Xuchang 461000, P. R. China

I. Supplementary Experiments

II. Supplementary Structure Figures

III. XPS, SEM, EDS, FT-IR Spectroscopy, UV-vis Spectroscopy, PXRD and TG

IV. Capacitive Performance Figures

V. Catalytic Oxidation Study

VI. Supplementary tables

VII. References

*Corresponding author. E-mail address: Houyj@xcu.edu.cn;

365063148@qq.com

I. Supplementary experiments

Materials and methods

We used chemicals that were commercially purchased without further purification $((NH_4)_6Mo_7O_{24}$/ptyz/$CuCl_2 \cdot 2H_2O$/$AgNO_3$/$NaSiO_3$ were purchased from Energy Chemical and J&K Chemicals; Methyl phenyl/1-Methyl-4-(methylthio) benzene/1-Methoxy -4-(methylthio) benzene/4-Chlorothioanisole/4-Fluorothioanisole/4-Nitrylhioanisole/benzyl sulfide /phenyl sulfide were purchased from Aladdin and Sigma-Aldrich). We detected the IR spectra using KBr pellets as the background in the range 400–4000 cm^{-1} on an Alpha Centaur FT/IR spectrophotometer. The PXRD patterns of the samples were recorded on a Rigaku Dmax 2000 X-ray diffractometer with graphite monochromatized Cu-Ka radiation ($\lambda = 0.154$ nm) and 2θ varying from 5° to 50°. The diffuse reflectivity spectra were performed on finely ground samples with a Cary 500 spectrophotometer equipped with a 110 mm diameter integrating sphere, which were measured from 200 to 800 nm. Cyclic voltammetry (CV), galvanostatic charge−discharge (GCD) measurements, and electrochemical impedance spectroscopy (EIS) were carried out on a CHI660E electrochemical workstation. The GC analysis was performed with an Agilent HP6890 spectrometer with a flame ionization detector, which was used to monitor the conversion and selectivity. GC−MS at the final time point was used to confirm the identity of the

products. The GC−MS spectra were measured on an Agilent HP6890/5973MSD spectrometer.

General methods of electrochemical measurements.

The electrochemical performance was measured on a CHI660E electrochemical workstation in 0.1 M H_2SO_4 solution with traditional three-electrode system. Then, the CC was dried under vacuum after adding 100 μL of N-methylpyrrolidone. The Ag/AgCl (3 M KCl) electrode was acted as a reference electrode, and a Pt wire was used as the counter electrode.

General methods for the selective oxidation of MPS

MPS oxidation: MPS (0.25 mmol), catalysts (2.5 μmol), oxidant (30% H_2O_2, 0.4 mmol), internal standard (Naphthalene, 0.25 mmol) and solvent (Methanol: 0.5 mL) were mixed in the reaction vessel. The catalytic reaction was carried out at 60 ℃. After the catalytic reaction was finished, GC-FID and GC-MS were used to analyze and identify the resulting mixture.

X-ray crystallography

A Bruker Smart CCD diffractometer with Mo Kα radiation (λ = 0.71073 Å) was used to collect the crystallographic data of four compounds at 293 K or 220 K by θ and ω scan modes. The method of empirical absorption correction was adopted. SHELXTL-97 software was used to solve the structures of **1-3** and refine the data.[1] In **1-3**, most non-H atoms are refined anisotropically, and only some of water molecules were excepted. H atoms linked to the C and N atoms were were fixed in their ideal

positions. To get reasonable thermal parameters and atom sites, some commands such as "isor" and "dfix" were utilized.

The CCDC reference numbers for compounds **1-3** are 2295785- 2295787
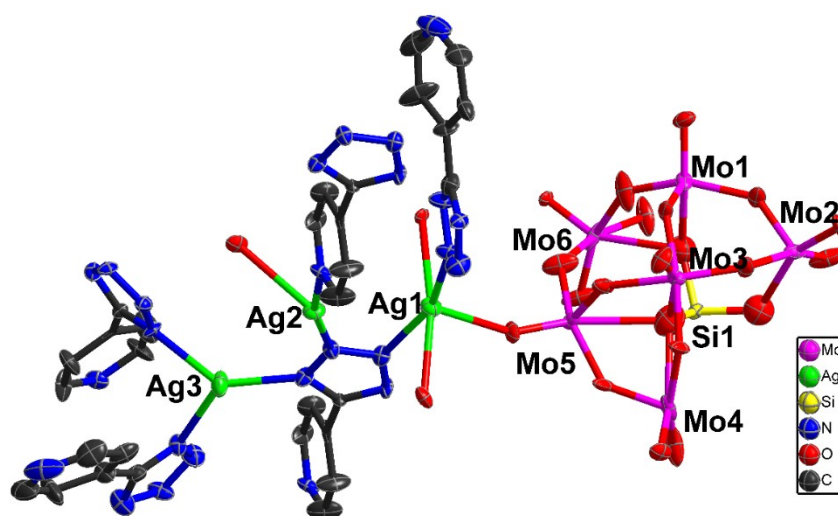
II. Supplementary Structure Figures

Fig. S1 ORTEP drawing of **1** with thermal ellipsoids at 50% probability. Free water molecules are omitted for clarity. (Color code: Mo, purple; Si, yellow; Ag, green; O, red; N, blue; C, black.).
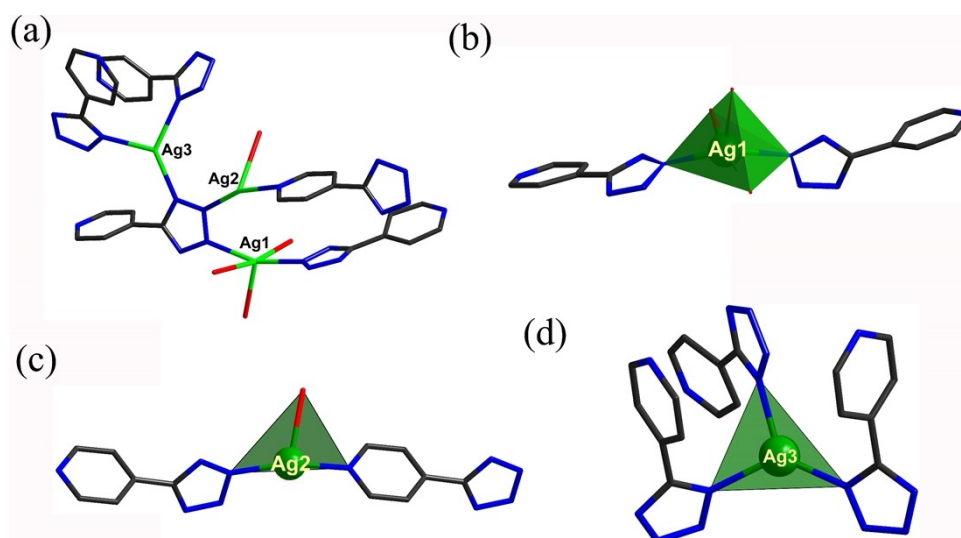

Fig. S2 (a) Ball and stick representation of the Ag-pytz subunit in POMCP **1**; (b)

Tenta-coordinated tetragonal geometry of Ag1; (c) Three-coordinated triangle geometry of Ag2; (d) Tix-coordinated triangle geometry of Ag3 in **1**. The Ag–N bond lengths are in the range from 2.169(8)-2.333(8) Å, and the N-Ag-N angle is 101.2(3)-162.6(3).
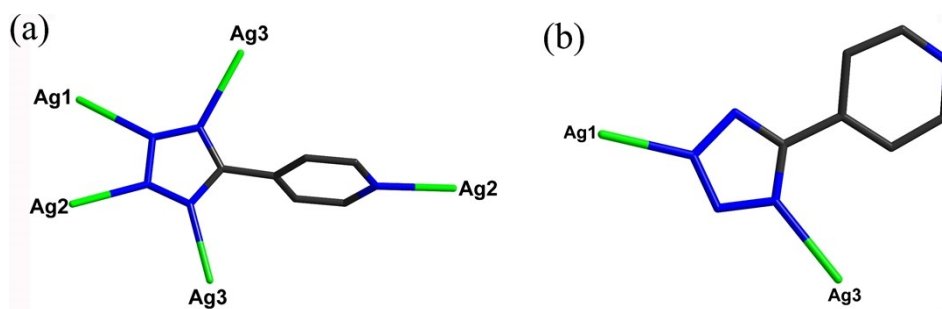

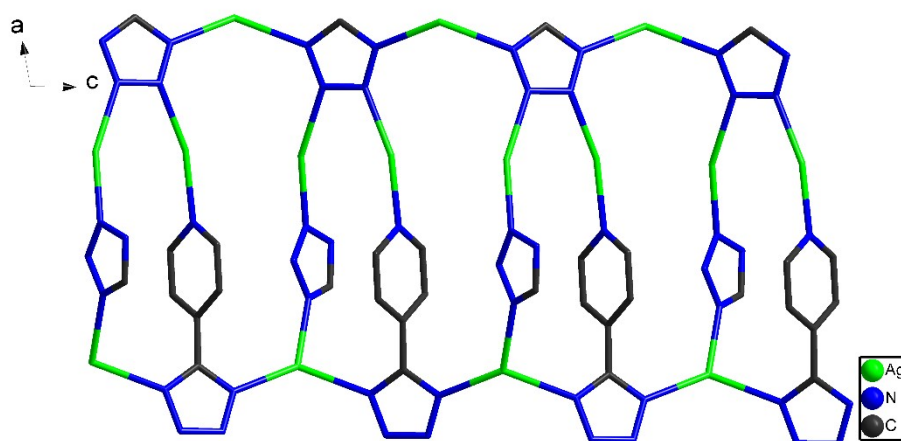**Fig. S3** (a and b) The coordination modes of bty ligands in **1**.

Fig. S4 view of 1D chain constructed from {Ag$_3$pytz$_3$} and {Ag$_4$ptyz$_4$} in **1**.
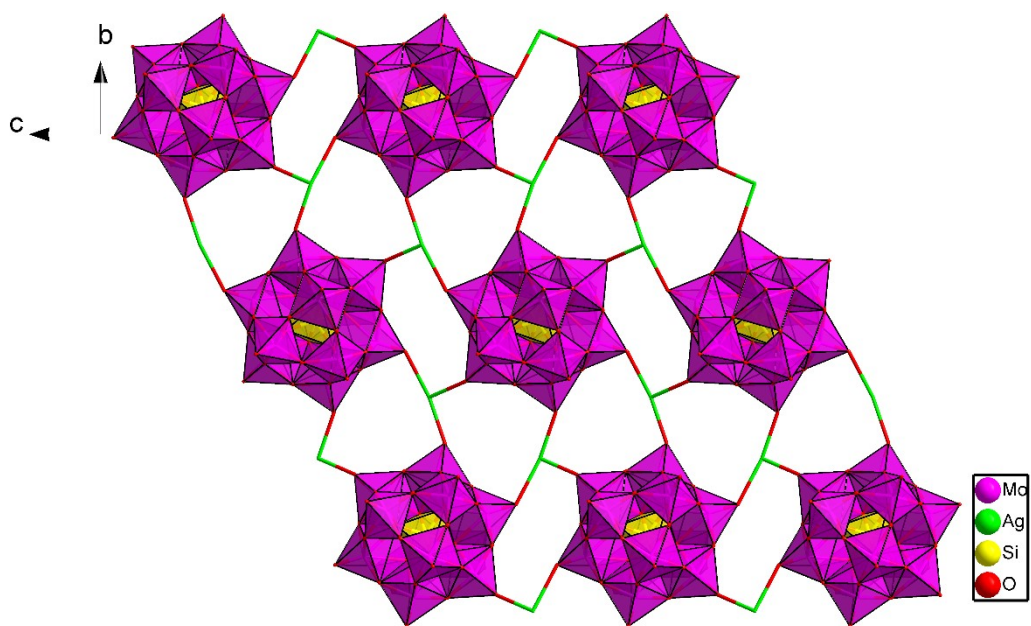
Fig. S5 view of 2D sheet constructed from {SiMo$_{12}$} and Ag ion in **1**.
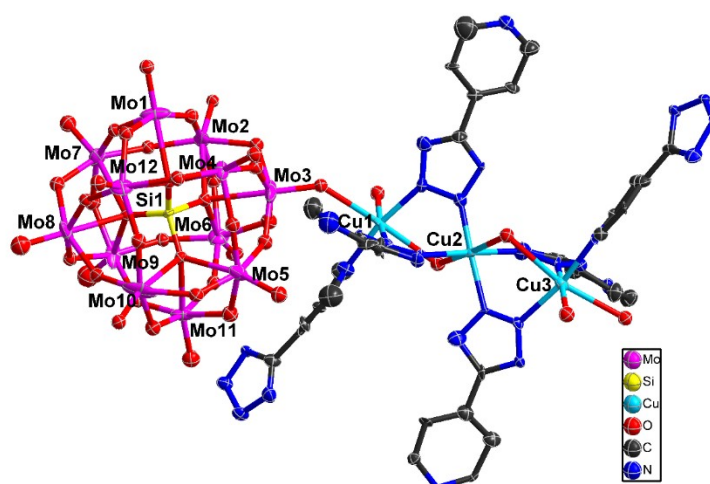

Fig. S6 ORTEP drawing of **2** with thermal ellipsoids at 50% probability. Free water

molecules are omitted for clarity. (Color code: Mo, purple; Si, yellow; Cu, light blue;
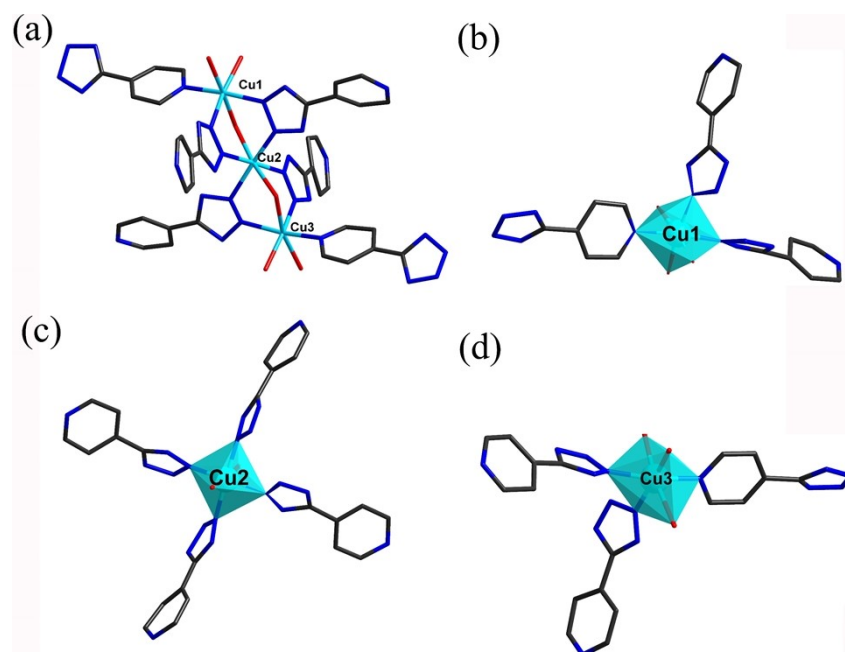
O, red; N, blue; C, black.).

Fig. S7 (a) Ball and stick representation of the Cu-pytz subunit in POMCP **2**; (b) Six-coordinated octahedral geometry of Cu1; (c) Six-coordinated octahedral geometry of Cu2; (d) Six-coordinated octahedral geometry of Cu3 in **2**. The Cu–N bond lengths are in the range from 1.87(3)-2.08(3) Å, and the N-Cu-N angle is 89.8(13)-178.1(19)°.
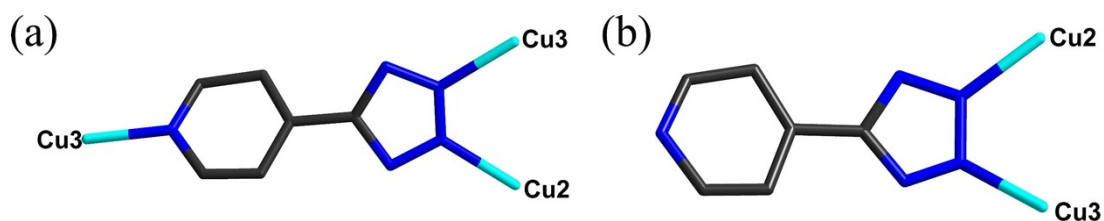

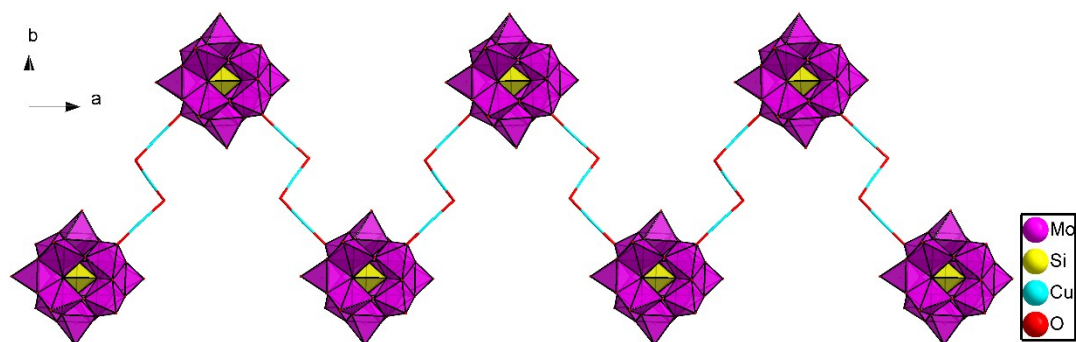**Fig. S8** (a and b) The coordination modes of pytz ligands in **2**.

Fig. S9 view of 1D chain constructed from {SiMo$_{12}$} and Cu ionin compound **2**.
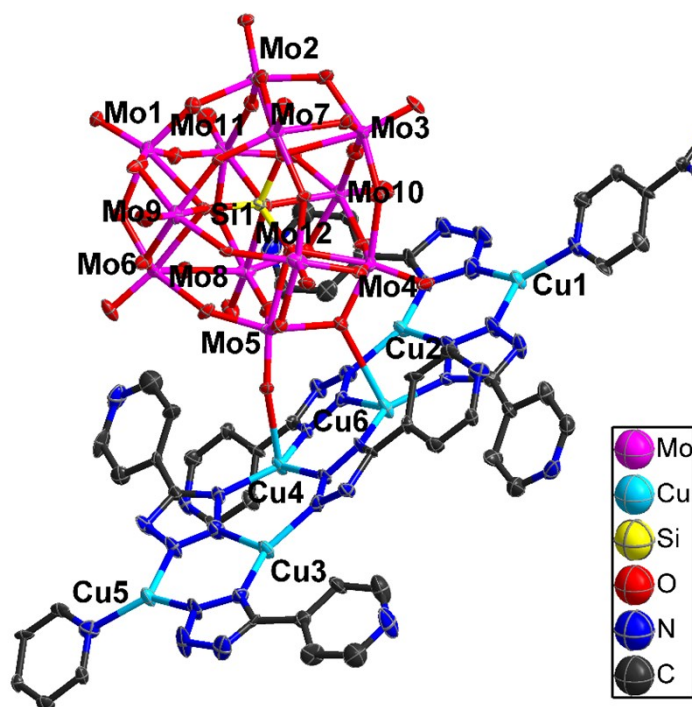
Fig. S10 ORTEP drawing of **3** with thermal ellipsoids at 50% probability. Free water molecules are omitted for clarity. (Color code: Mo, purple; Si, yellow; Cu, light blue; O, red; N, blue; C, black.).
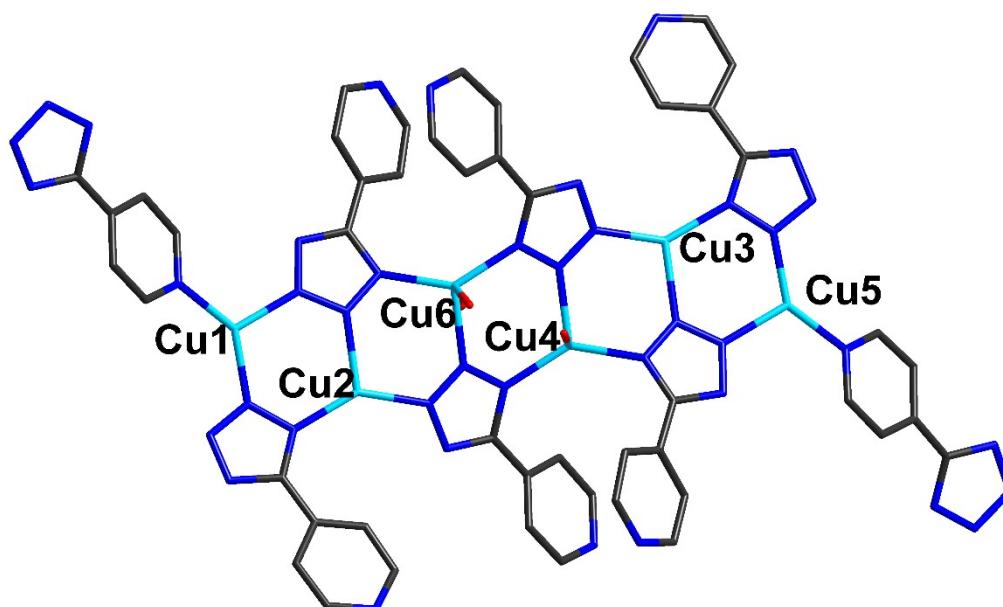

Fig. S11 Ball and stick representation of the Cu-pytz subunit in POMCP **3**.
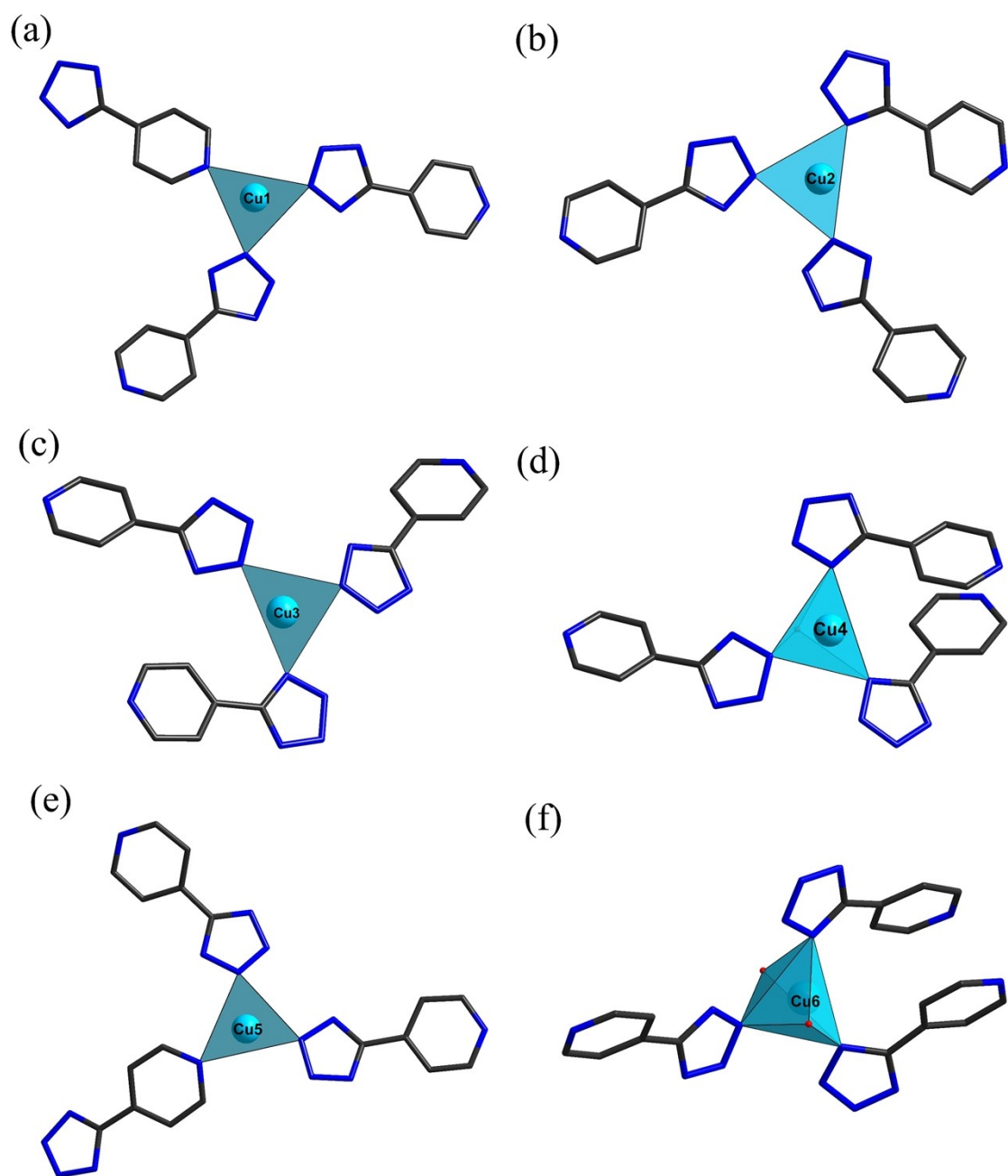
Fig. S12 (a) Three-coordinated triangle geometry of Cu1; (b) Three-coordinated triangle geometry of Cu2; (c) Three-coordinated triangle geometry of Cu3; (d) Tetra - coordinated tetrahedron geometry of Cu4; (e) Three-coordinated triangle geometry of Cu5; (f) penta-coordinated tetragonal geometry of Cu6 in **3**. The Cu–N bond lengths are in the range from 1.913(11)-2.133(11) Å, and the N-Cu-N angle is 106.4(4)-143.0(5)°.
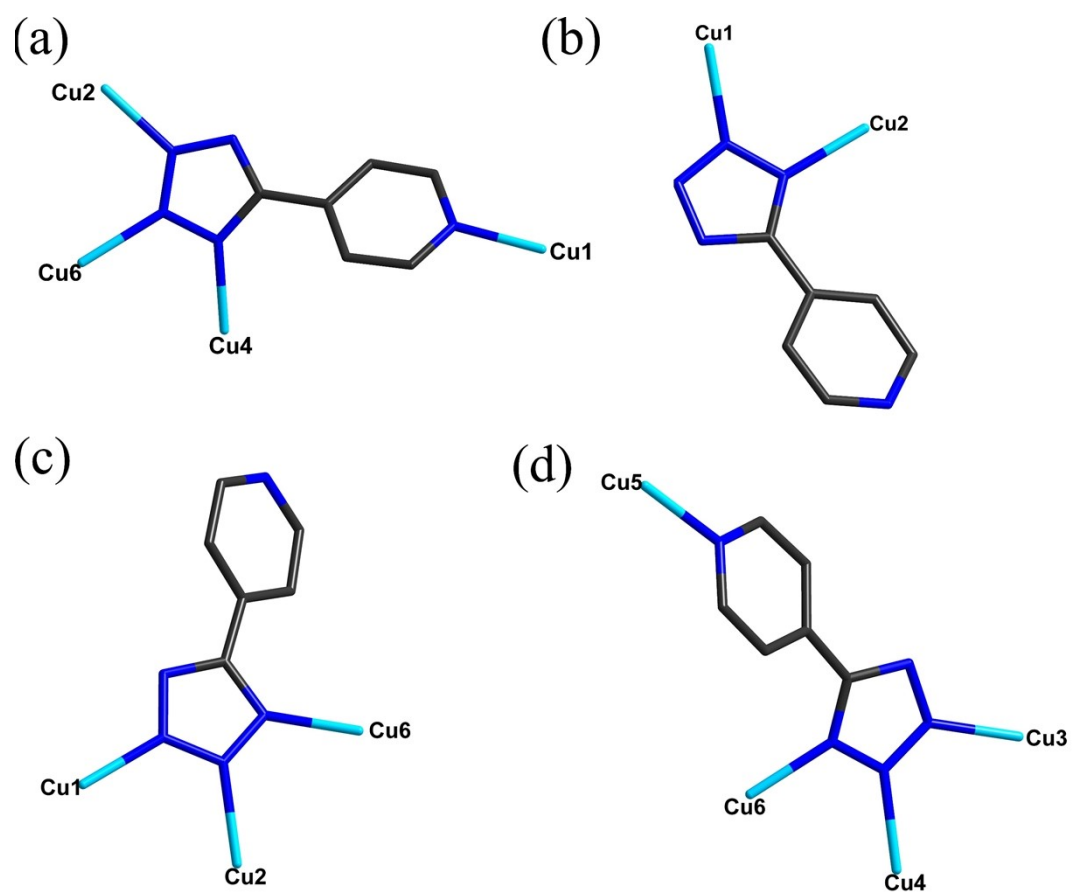
Fig. S13 (a, b, c and d) The coordination modes of pytz ligands in **3.**

Fig. S14 (a) XPS full spectrum for compound **1**; (b) High-resolution scan of C1s electron in compound **1**; (c) High-resolution scan of O1s electron in compound **1**; d) High-resolution scan of Si2p electron in compound **1**; (e) High-resolution scan of Ag3d electron in compound **1**; (f) High-resolution scan of Mo3d electron in compound **1**.
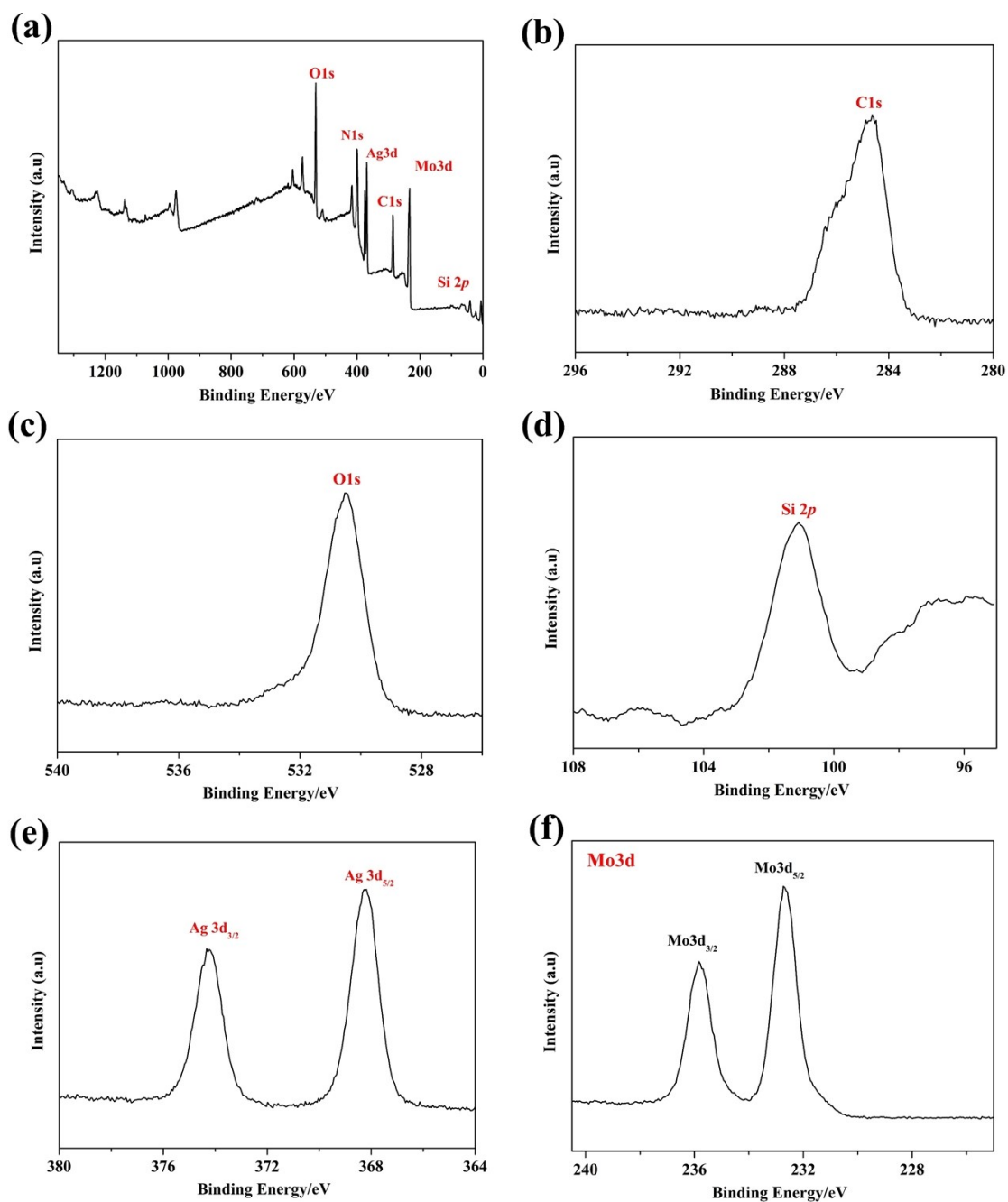
Fig. S15 (a) XPS full spectrum for compound **2**; (b) High-resolution scan of C1s electron in compound **2**; (c) High-resolution scan of O1s electron in compound **2**; d) High-resolution scan of Si2p electron in compound **2**; (e) High-resolution scan of Cu2p electron in compound **2**; (f) High-resolution scan of Mo3d electron in compound **2**.
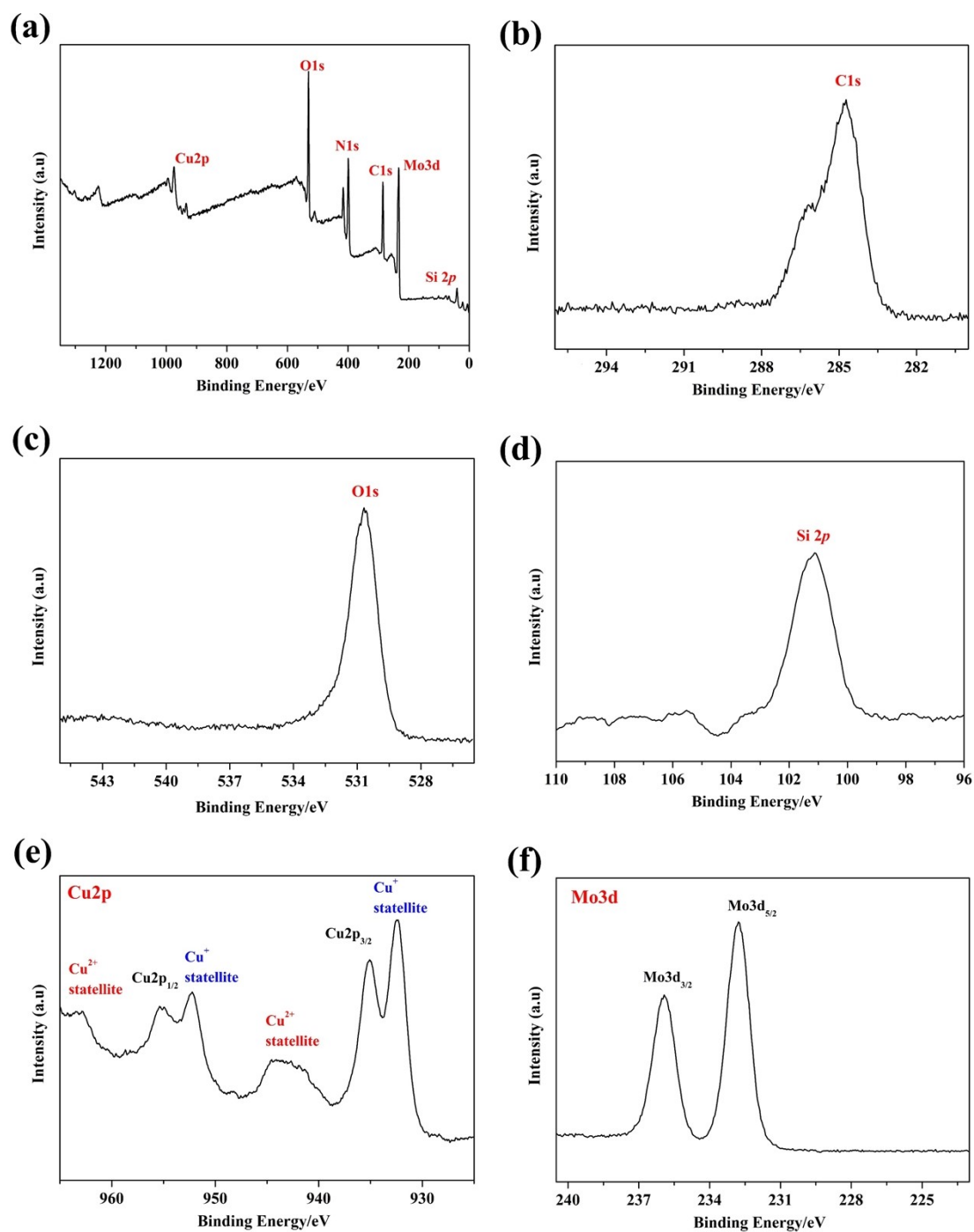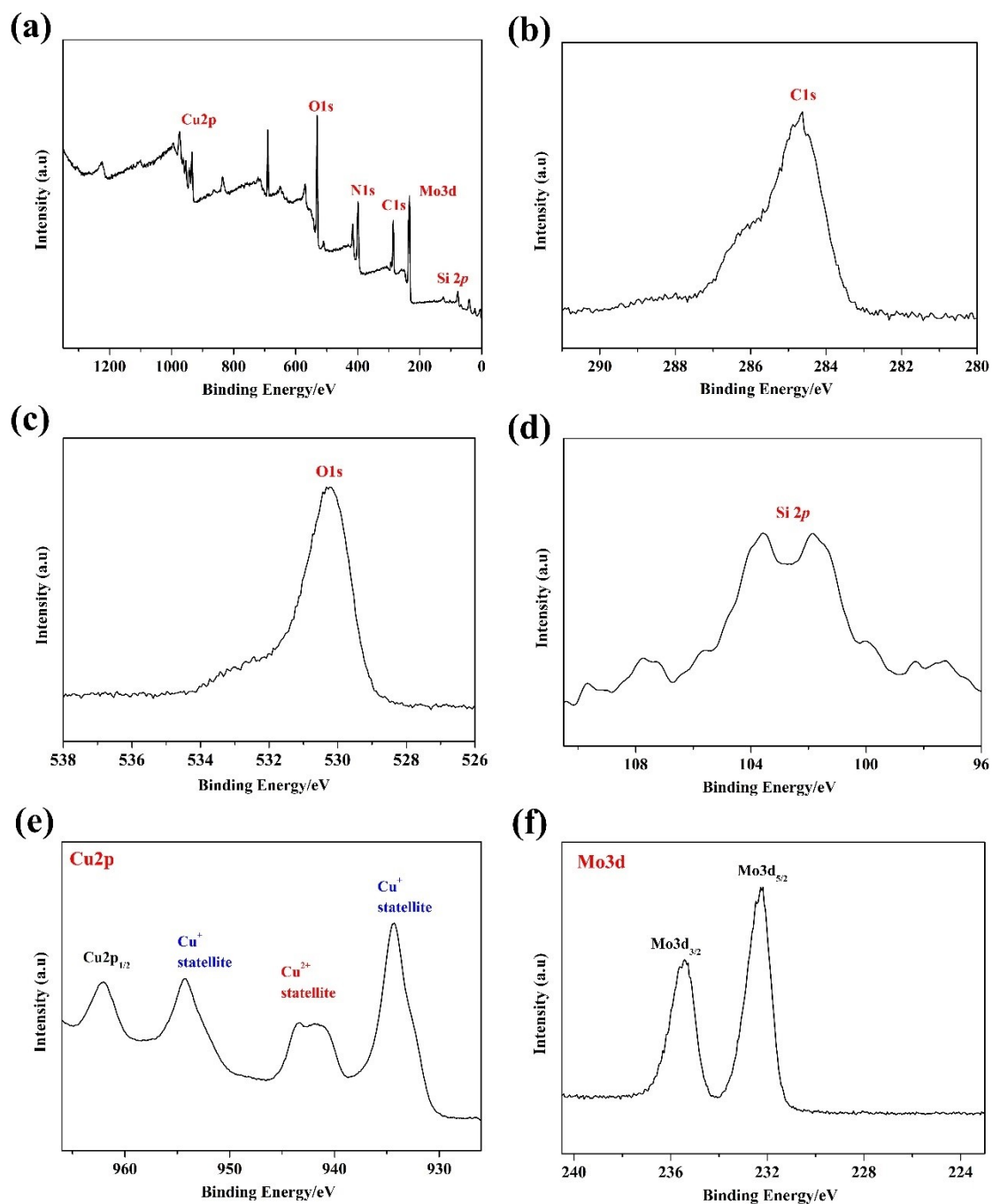
Fig. S16 (a) XPS full spectrum for compound **3**; (b) High-resolution scan of C1s electron in compound **3**; (c) High-resolution scan of O1s electron in compound **3**; d) High-resolution scan of Si2p electron in compound **3**; (e) High-resolution scan of Cu2p electron in compound **3**; (f) High-resolution scan of Mo3d electron in compound **3**.

III. SEM, EDS, FT-IR Spectroscopy, UV-vis Spectroscopy and PXRD

Fig. S17 (a) SEM image of compound **1**; (b) EDS spectrum of compound **1**; (c-h) EDX elemental mapping of Mo, O, Ag, C, Si and N in compound **1**.
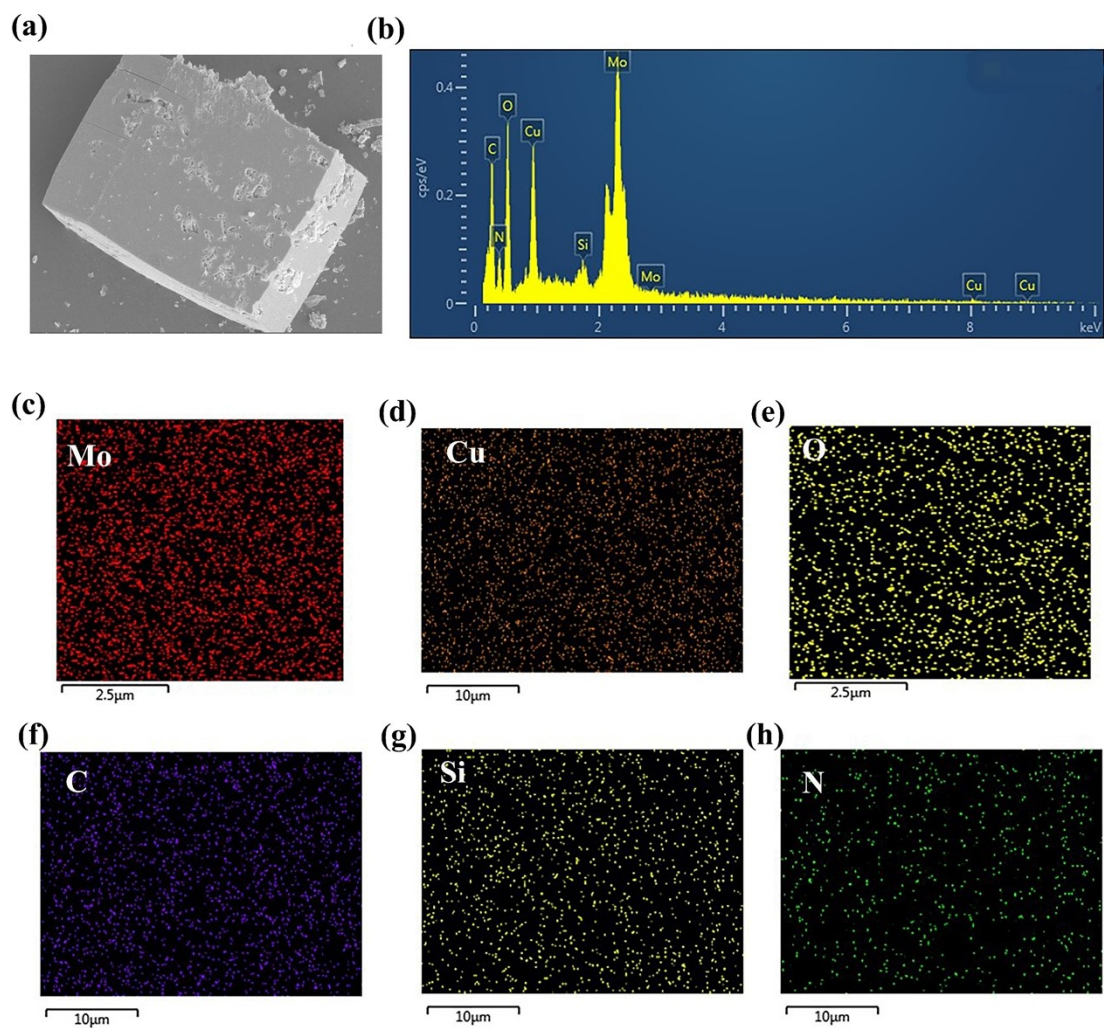
Fig. S18 (a) SEM image of compound **2**; (b) EDS spectrum of compound **2**; (c-h) EDX elemental mapping of Mo, Cu, O, C, Si and N in compound **2**.
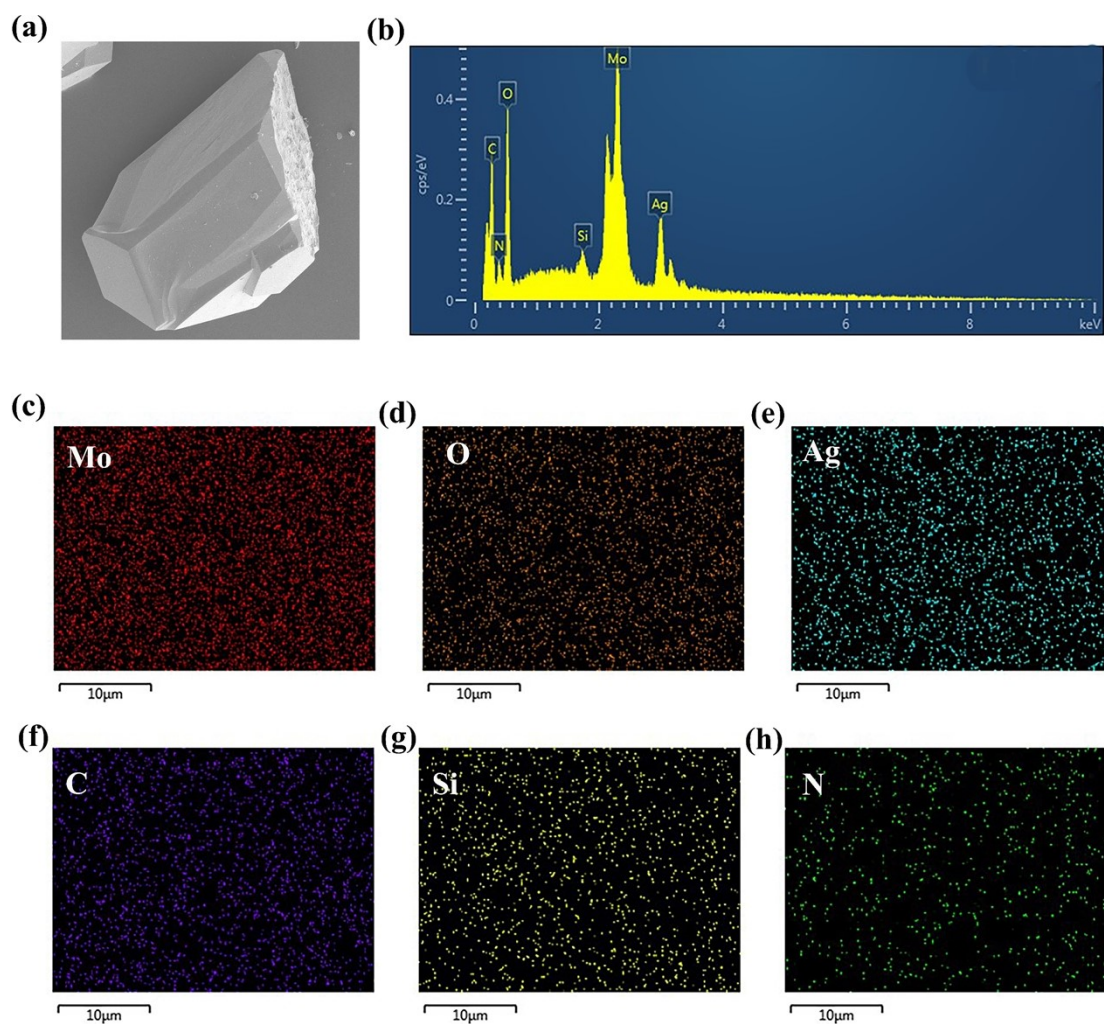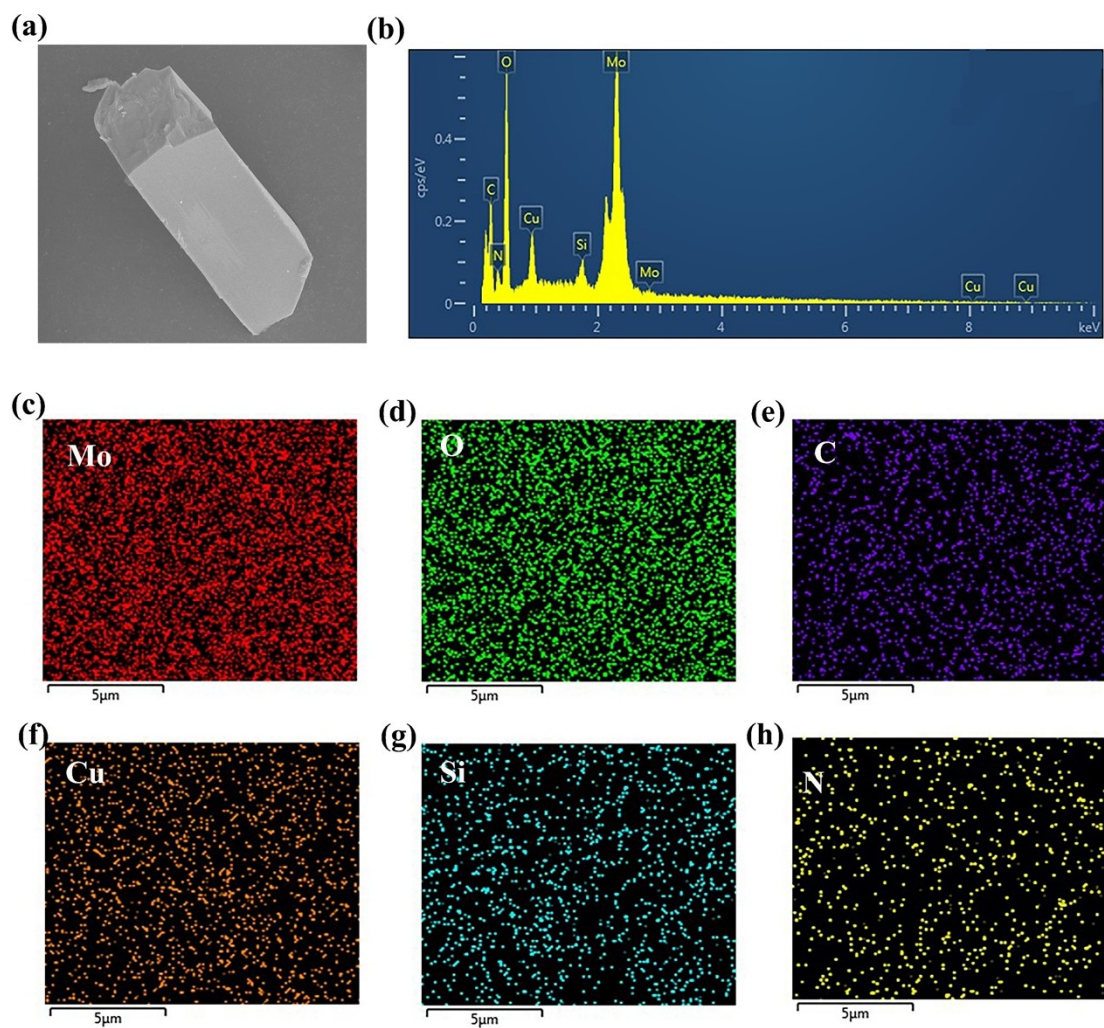
Fig. S19 (a) SEM image of compound **3**; (b) EDS spectrum of compound **3**; (c-h) EDX elemental mapping of Mo, O, C, Cu, Si and N in compound **3**.
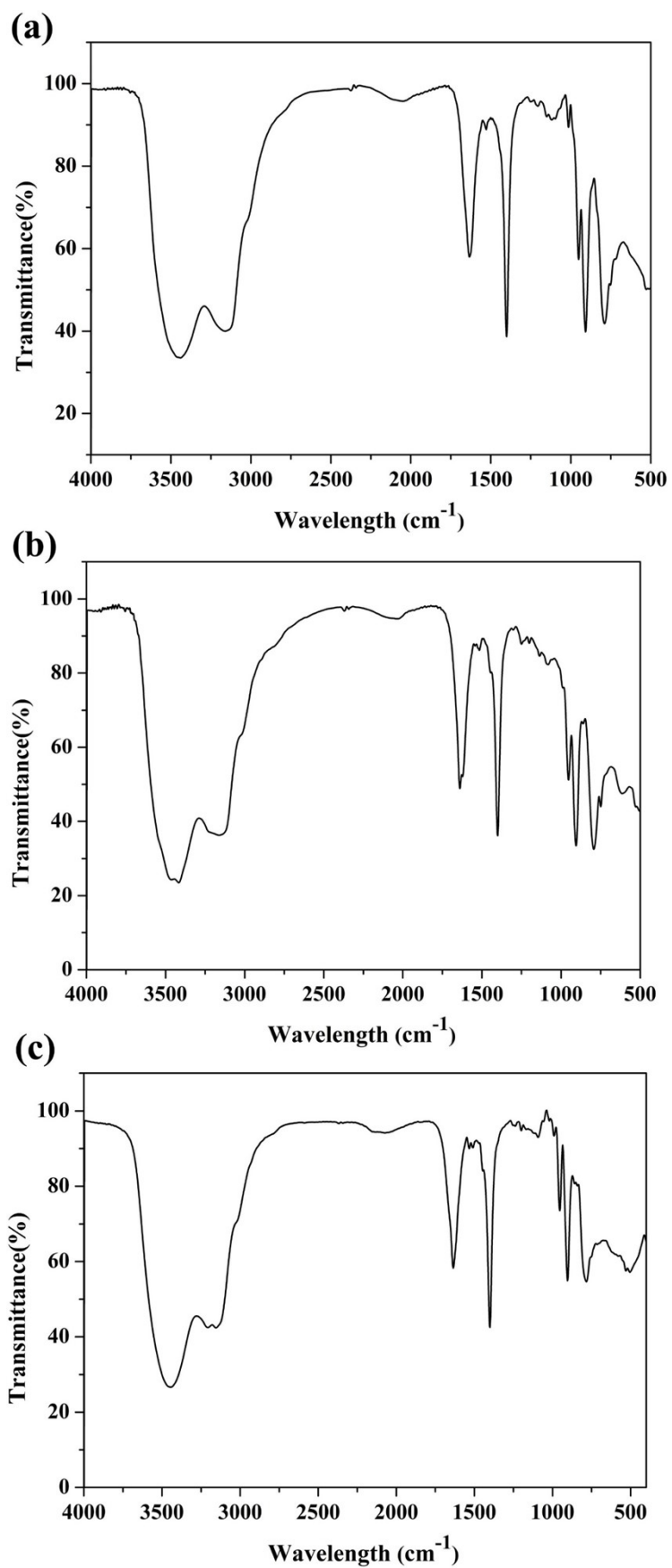
Fig. S20 IR spectra for compounds **1-3**.
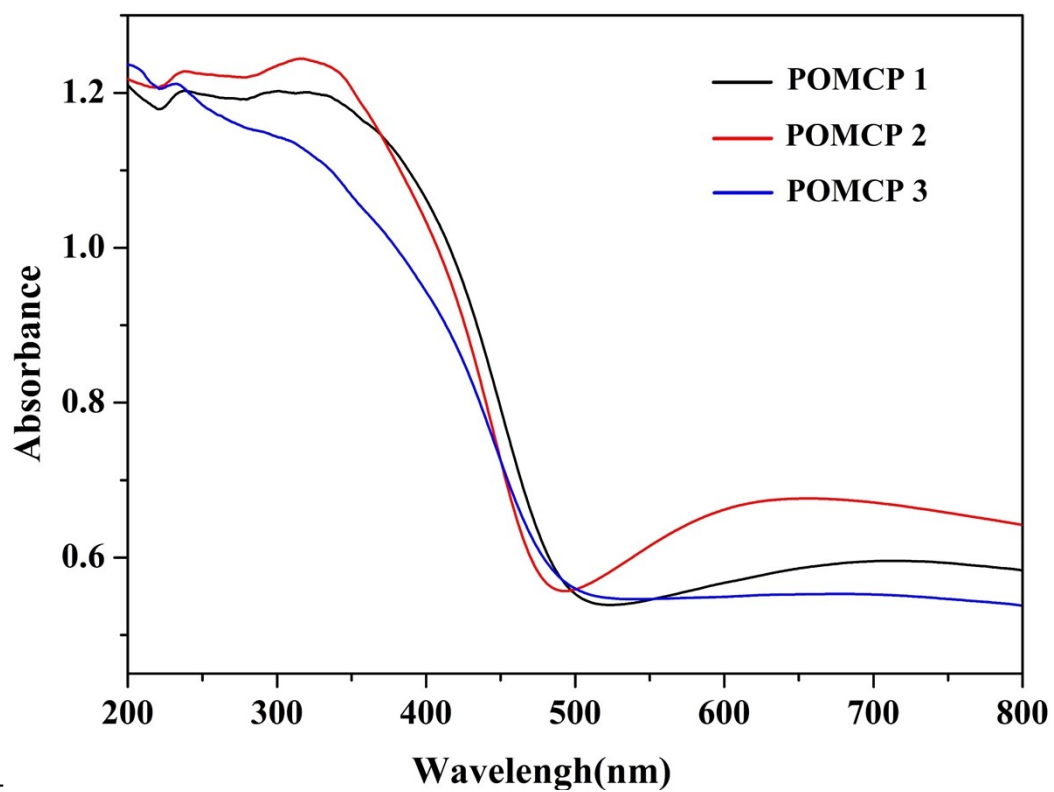
Fig. S21 UV−vis diffuse reflectance spectra of compounds **1-3**.
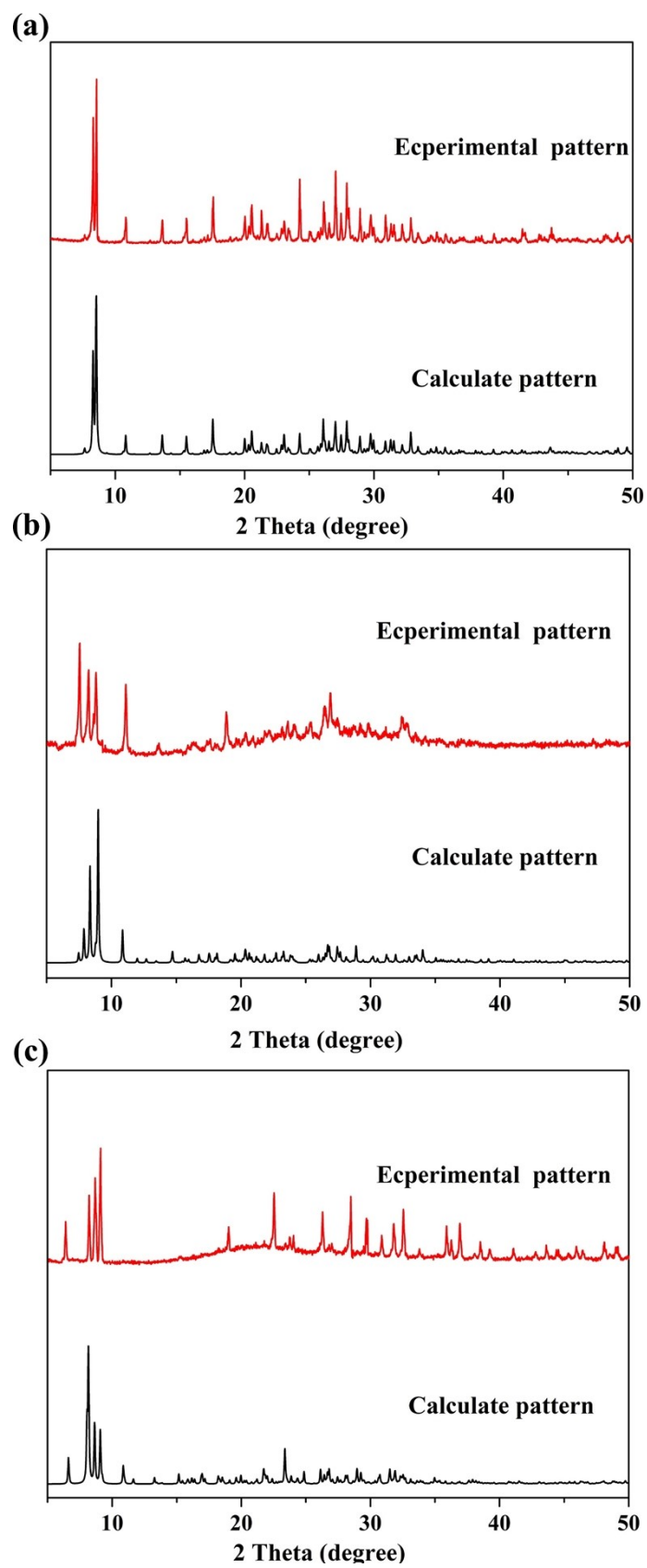
Fig. S22 (a, b and c) The calculated and experimental PXRD patterns for compounds

1-3.
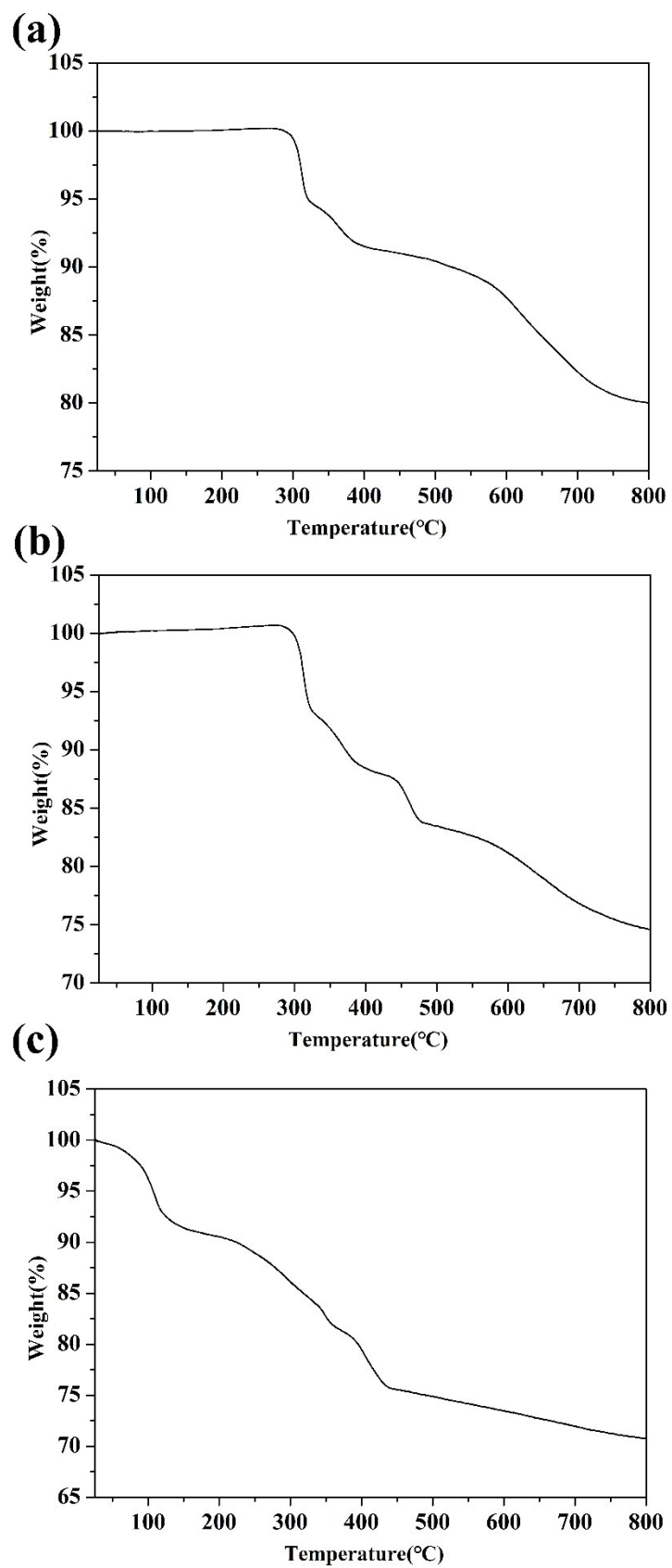
Fig. S23 Thermogravimetric plots of compounds **1-3**, which exhibited multistep

weight loss processes.

IV. Capacitive Performance Figures
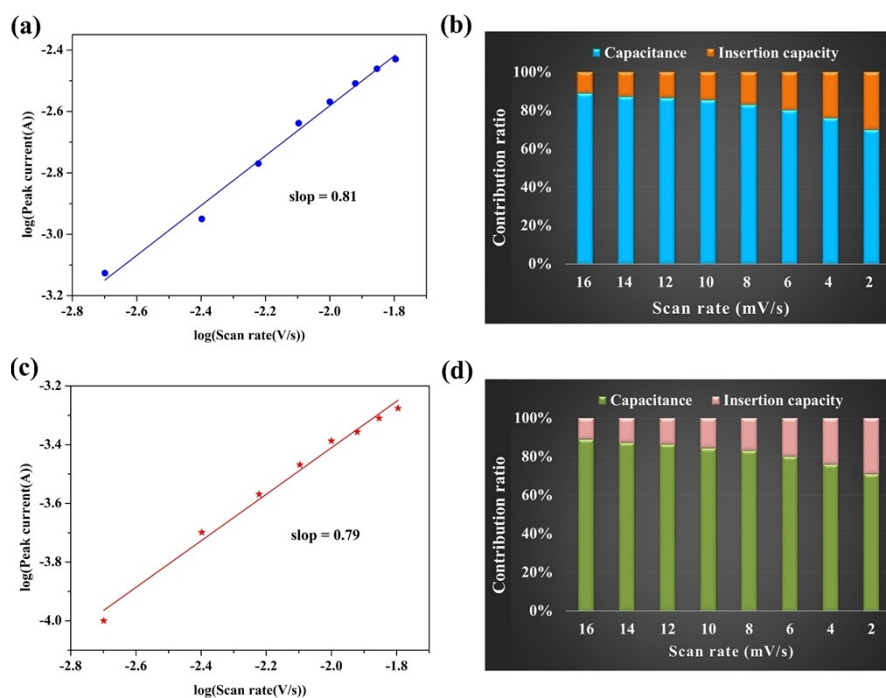
Fig. S24 (a and c) Fitting b-value of the peak currents of compound **2** and **3**; (b and d)

Contribution ratio of the capacitive versus scan rate of compound **2** and **3**.
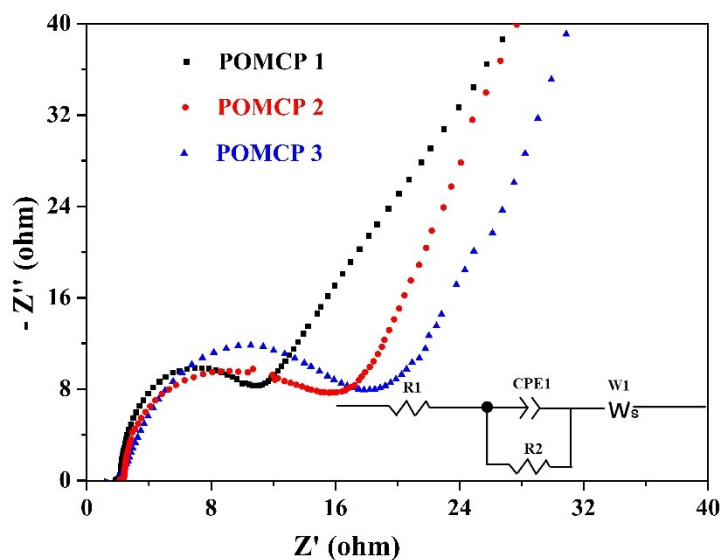
Fig. S25 EIS spectra POMCPs **1-3** based electrodes and the equivalent circuit of

electrochemical impedance spectra of sulfur composite cathodes (one semicircle is

ascribed to charge-transfer resistance (R2), and the Warburg resistance (Ws) locates

in the tail line.)
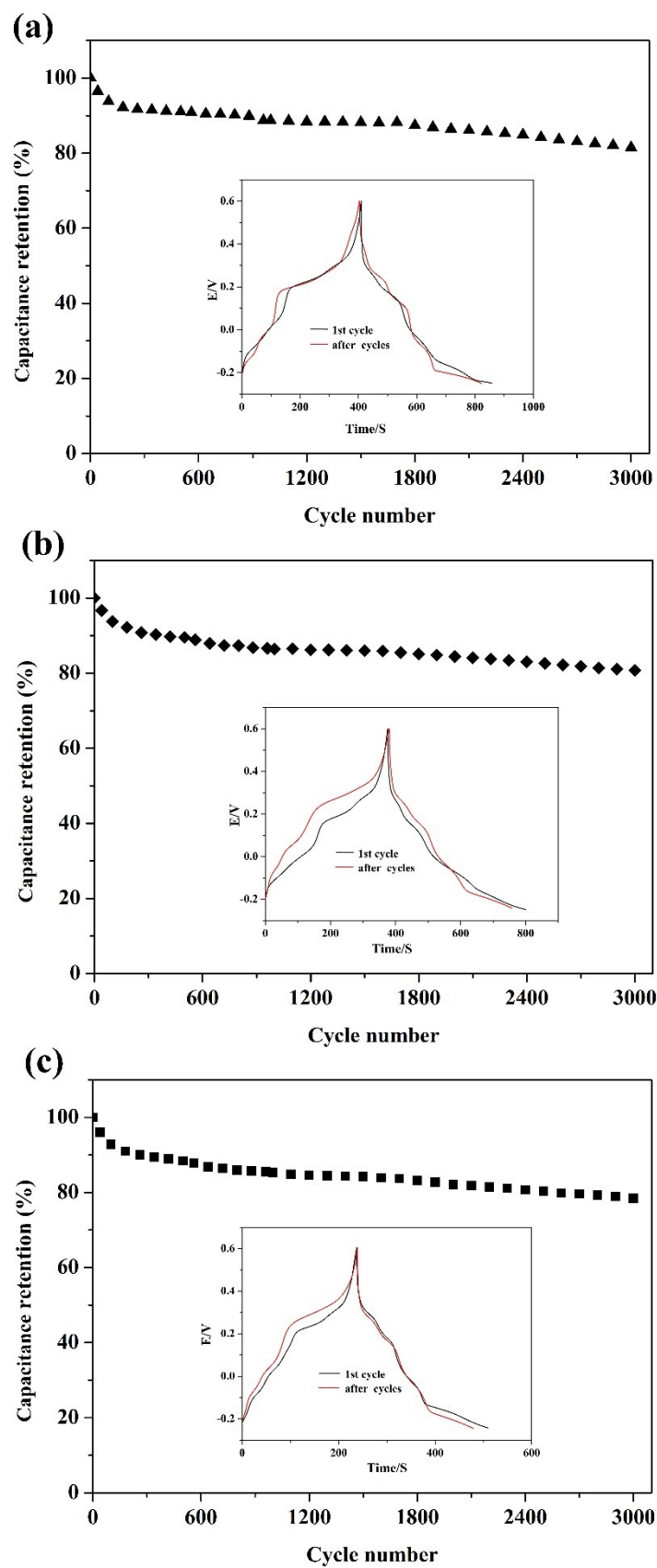
Fig. S26 Cyclic stabilities of electrodes based on **1**(a), **2**(b) and **3**(c) after 3000

cycles.

V. Catalytic Oxidation Study

(a)

(b)
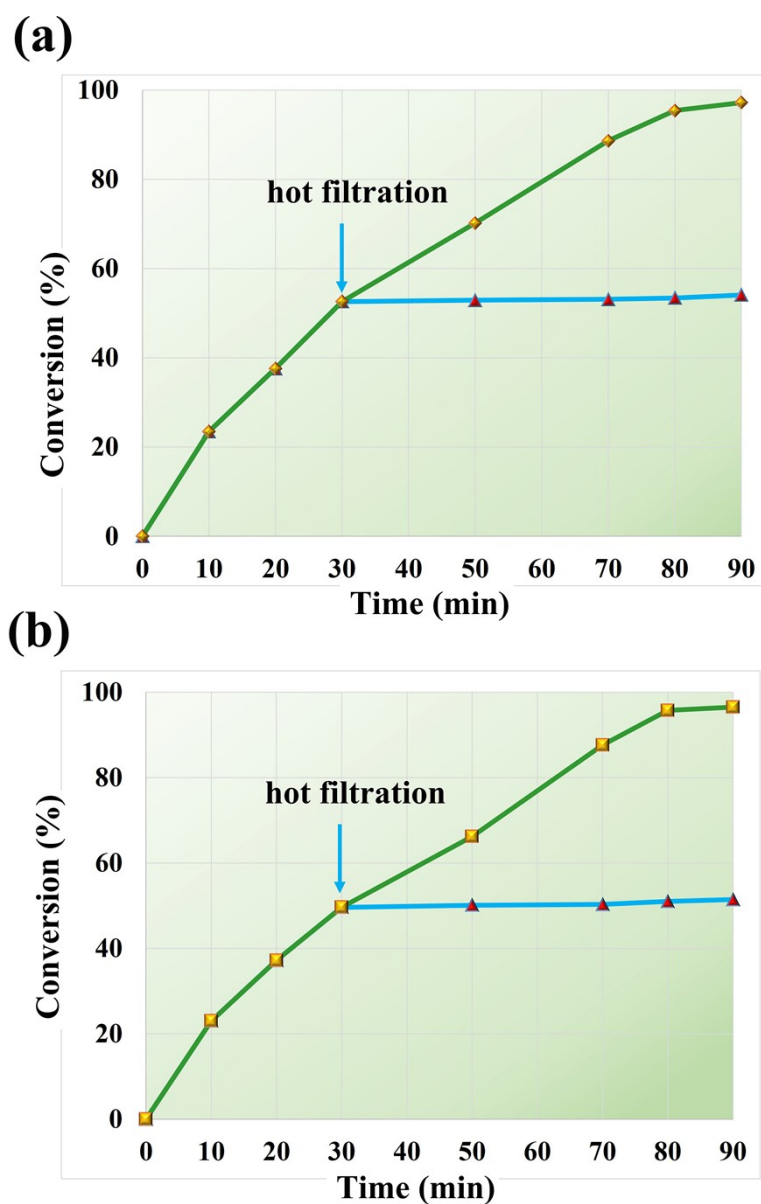
Fig. 27 The conversion of MPS oxidation for compounds **2** and **3** and the hot filtration test for the oxidation of MPS.

(a)

y=-0.04398x+0.27937
R^2=0.98795

(b)

y=-0.03576x+0.21699
R^2=0.96077
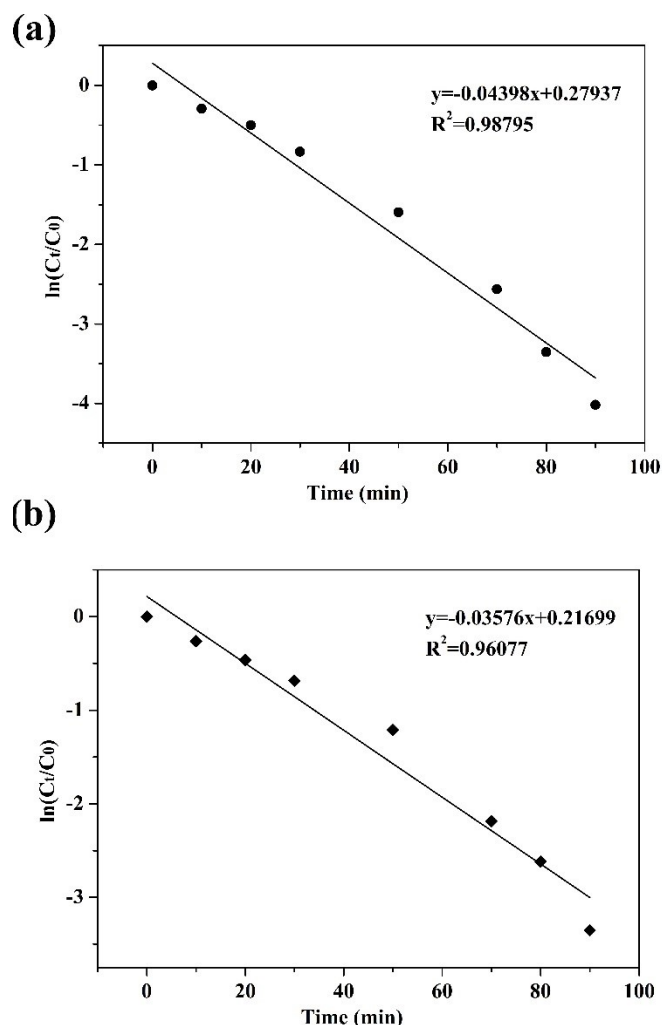
Fig. S28 (a and b) Kinetic analysis of MPS oxidation for compounds **2** and **3** ($\ln(C_t/C_0)$ versus reaction time, C_t and C_0 represent the concentration of MPS at some time and the starting time).
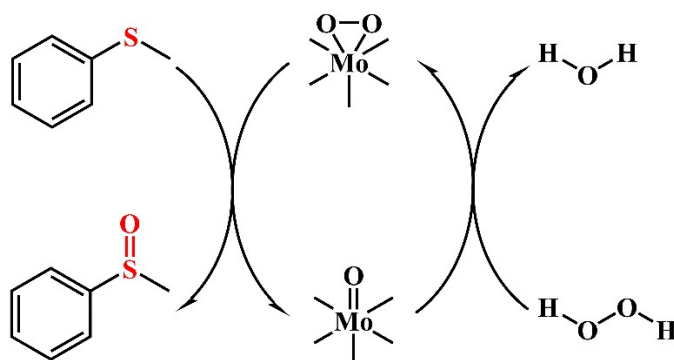
Fig. S29 Catalytic oxidation pathway of MPS to MPSO and methyl phenyl sulfone (MPSO$_2$).
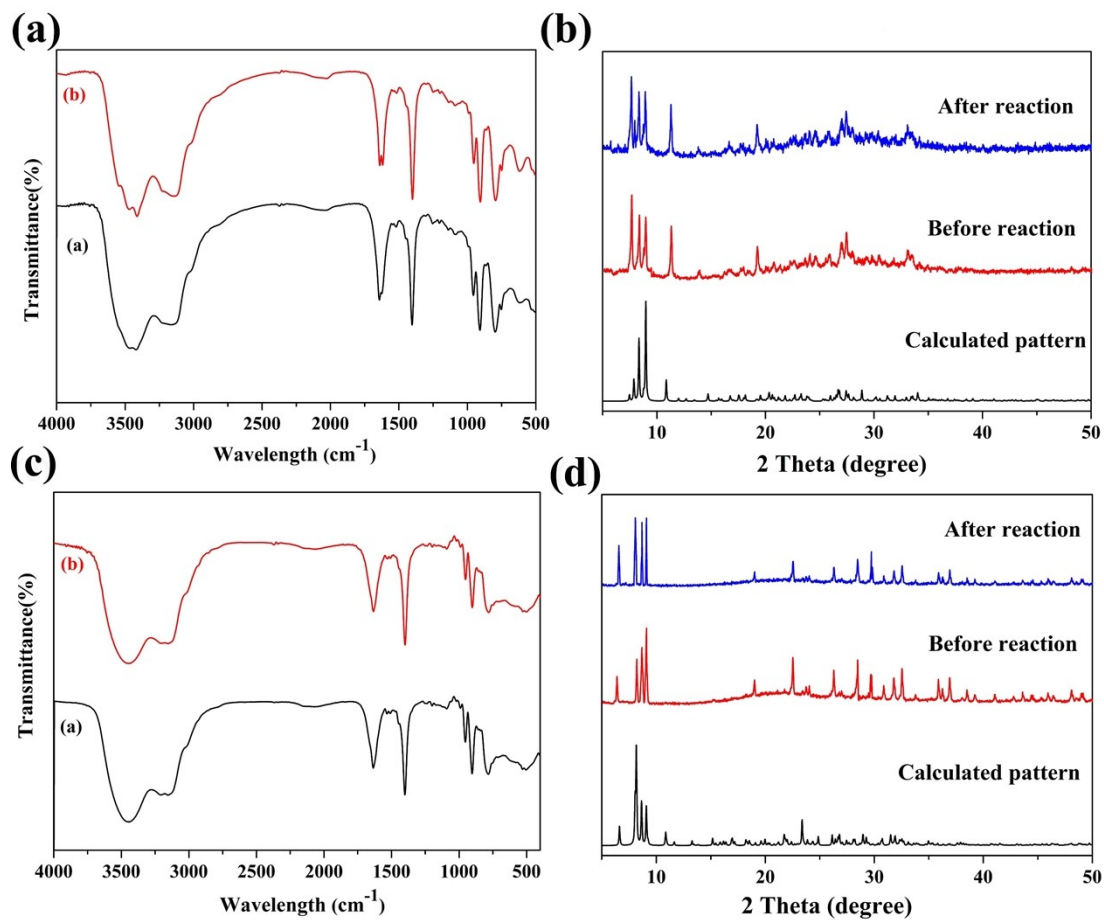
Fig. S30 (a, and c) IR spectra for **2** and **3**; (b and d) PXRD patterns for **2** and **3** before and after catalysis. In the IR spectra, the black and red lines represent the infrared absorption curves of the fresh catalyst and the catalyst recovered after the reaction, respectively. In the PXRD patterns, the red and blue lines represent PXRD patterns of the fresh catalyst and the catalyst recovered after the reaction, respectively, and the black curve is the simulated value.
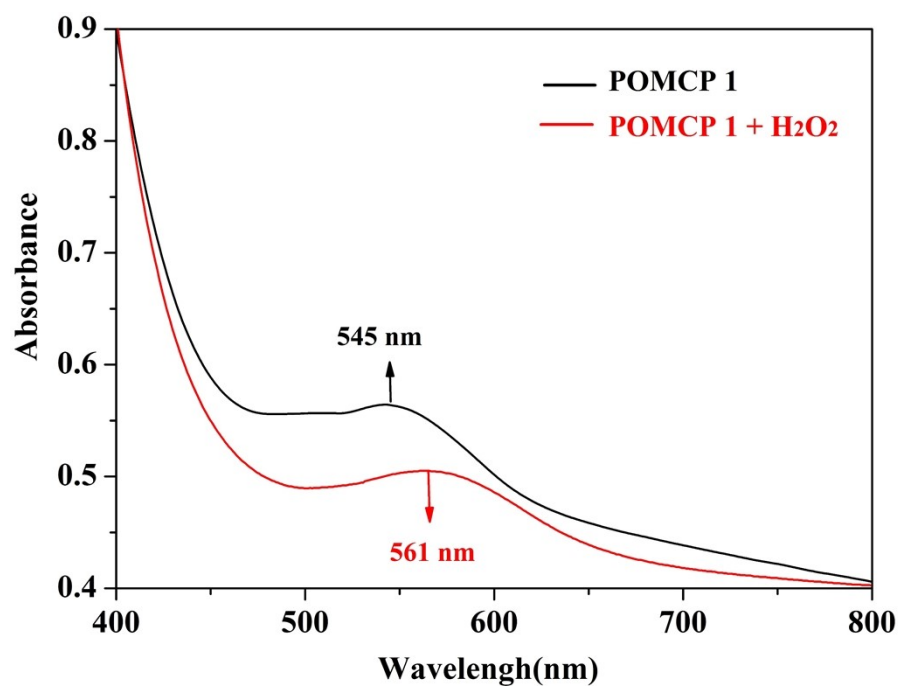
Fig. S31 UV-vis spectra of POMCP **1** in DMSO with one-drop portion of H_2O_2 in the visible region.

VI. Supplementary tables

Table S1. Some POM-based hybrids as electrodes materials of supercapacitors.

Electrode	$C_S(F \cdot g^{-1})$	Current density$(A \cdot g^{-1})$	ref
POMCP **1**	261.76	0.5	This work
POMCP **2**	248.82	0.5	This work
POMCP **3**	156.47	0.5	This work
$[Cu_3(bty)_3][BW_{12}O_{40}]$❿$4H_2O$	214.59	0.48	2
$[Cu_{2.5}(bty)_5][BW_{12}O_{40}]$❿$7H_2O$	189.17	0.48	2
$[Ag_{10}(C_2H_2N_3)_8][HVW_{12}O_{40}]$	93.5	1.5	3
$[AgH_2(imbta)_2](PMo_{12}O_{40})$	320	1	4
$[Co^{II}(pzta)_2(H_2O)]_2(H_4GeMo_{12}O_{40}) \cdot 4H_2O$	182	1	5
$[Cu^I(btx)]_4[SiW_{12}O_{40}]$	110.3	3	6
$(H_2bpe)(Hbpe)_2\{[Cu(pzta)(H_2O)][P_2W_{18}O_{62}]\} \cdot 5H_2O$	168	5	7
$[Ru(bpy)_3]_{3.33}P_2Mo_{18}O_{62} \cdot mH_2O$	125	0.2	8
$[Ru(bpy)_3]_3P_2Mo_{18}O_{62} \cdot nH_2O$	68	0.2	8
$CoK_4[P_2W_{18}O_{62}]@Co_3(btc)_2$	490.7	1	9
$H\{Zn_4(DIBA)_5(HPO_2)]_2(\alpha\text{-}PMo_8Mo_4O_{40}Zn_2)\}$	171.17	0.5	10
$Ag_5(C_2H_2N_3)_6][H_5 \subset SiMo_{12}O_{40}]$	155.0	0.5	11
$[Cu_4H_2(btx)_5(PW_{12}O_{40})_2] \cdot 2H_2O$	100.0	2	12

Table S2. Catalytic Activity of Different Catalysts for the Oxidation of MPS

Entry	Ca	Con (%)	Sel (%)[b]	Rection System
1	{SiMo$_{12}$}	73.6	66.5	Homogeneous
2	AgNO$_3$	69.5	62.3	Homogeneous
3	AgNO$_3$ + {SiMo$_{12}$}	77.8	70.5	Homogeneous
4	CuCl	65.4	59.3	Homogeneous
5	CuI + {SiMo$_{12}$}	70.6	68.2	Homogeneous
6	CuCl$_2$	66.5	58.6	Homogeneous
7	{SiMo$_{12}$} + CuCl$_2$	76.4	69.6	Homogeneous
8	POMCP **1**	98.5	99.1	Heterogeneous
9	POMCP **2**	97.2	96.8	Heterogeneous
10	POMCP **3**	96.5	97.2	Heterogeneous
11	Blank	29.4	47.3	*

[a]Reaction conditions: sulfide (0.25 mmol), catalysts (1 mol%), H$_2$O$_2$ (4 mmol), methanol (0.5 mL); [b]Selectivity to sulfoxides, the byproduct was sulfone.

Table S3. Crystal data and structure refinement for **1-3**.

Complex	1	2	3
formula	$C_{12}H_8SiAg_3N_{10}O_{20}Mo_{12}$	$C_{48}H_{60}Si_2Cu_6N_{40}O_{91}Mo_{24}$	$C_{36}H_{28}SiCu_6N_{30}O_{42}Mo_{12}$
formula weight	3051.16	5393.34	3113.49
T (K)	296(2)	296(2)	296(2)
crystal system	Monoclinic	Monoclinic	Triclinic
space group	*P21/c*	*Cc*	*P1*
a (Å)	10.5645(17)	22.670(3)	12.1212(8)
b (Å)	23.139(4)	13.9099(19)	12.3376(8)
c (Å)	12.261(2)	20.391(3)	13.9050(9)
α (°)	90	90	99.5642(9)
β (°)	101.419(3)	98.872(2)	98.4242(9)
γ (°)	90	90	113.4205(8)
U (Å³)	2937.8(8)	6353.0(15)	1829.0(2)
Z	4	4	1
μ (mm⁻¹)	4.551	3.401	3.815
reflections collected	5170	12390	10999
independent reflections	3976	6599	8342
R(int)	0.0545	0.0559	0.0117
GOF on F^2	1.028	1.030	1.002
R_1^a [I> 2σ(I)]	0.0491	0.0838	0.0327
wR_2^b [I> 2σ(I)]	0.0913	0.1900	0.0818

Table S4. Selected distances (Å) and angles (˚) for **1-3**.

		Compound **1**	
Mo(1)-O(12)	1.872(17)	Mo (1)-O(22)	1.640(6)
Mo (2)-O(11)	2.042(15)	Mo (2)-O(20)	1.678(6)
Mo (3)-O(9)	1.915(16)	Mo (3)-O(8)	2.022(14)
Mo (4)-O(4)	2.140(11)	Mo (4)-O(21)	1.657(6)
Mo (5)-O(12)	2.052(16)	Mo (5)-O(2)	2.137(10)
Mo (6)-O(5)	2.010(14)	Mo (6)-O(4)	1.969(12)
Si(1)-O(1)	1.563(10)	Si(1)-O(2)	1.723(10)
Ag(1)-O(20)	2.473(6)	Ag(2)-N(8)	2.178(6)
O(1)-Si(1)-O(3)	115.3(5)	O(2)-Si(1)-O(4)	105.0(5)
		Compound **2**	
Mo(1)-O(24)	1.67(3)	Mo (2)-O(4)	1.95(2)
Mo (3)-O(14)	2.31(2)	Mo (4)-O(6)	2.10(2)
Mo (5)-O(26)	1.90(2)	Mo (6)-O(34)	1.68(3)
Mo (7)-O(32)	2.00(3)	Mo (8)-O(3)	1.71(3)
Mo (9)-O(26)	1.85(2)	Mo (10)-O(5)	1.88(2)
Mo (11)-O(14)	2.33(2)	Mo (12)-O(5)	1.95(2)
Si(1)-O(18)	1.56(2)	Si(1)-O(14)	1.72(3)
Cu(3)-N(3)	2.08(2)	Cu(1)-N(1)	2.042(14)
O(18)-Si(1)-O(21)	113.6(12)	O(21)-Si(1)-O(9)	108.5(13)
		Compound **3**	
Mo(1)-O(2)	1.669(10)	Mo (2)-O(13)	1.948(8)
Mo (3)-O(35)	1.683(9)	Mo (4)-O(15)	1.831(9)
Mo (5)-O(19)	1.866(8)	Mo (6)-O(6)	1.887(7)
Mo (7)-O(3)	1.877(9)	Mo (8)-O(36)	1.674(9)
Mo (9)-O(37)	1.663(10)	Mo (10)-O(20)	1.991(8)
Mo (11)-O(5)	1.828(8)	Mo (12)-O(18)	2.059(8)
Si(1)-O(16)	1.594(8)	Si(1)-O(10)	1.678(7)
Cu(1)-N(3)	1.943(9)	Cu(2)-N(2)	1.953(8)
O(16)-Si(1)-O(9)	111.8(4)	O(7)-Si(1)-O(10)	107.1(4)

VII. References

1 a) G. M. Sheldrick, *SHELXL 97, Program for Crystal Structure Refinement, University of Gőttingen,* Germany, 1997; b) G. M. Sheldrick, *SHELXL 97, Program for Crystal Structure Solution, University of Gőttingen*, Germany.

2 Y. J. Hou, P. L. Han, L. K. Zhang, H. Li, Z. H. Xu, pH-controlled Assembling of POM-based Metal–organic Frameworks for Use as Supercapacitors and Efficient Oxidation Catalysts for Various Sulfides. *Inorg. Chem. Front.*, 2023, **10**, 148–157.

3 Y. Hou, H. J. Pang, C. J. Gómez-García, H. Y. Ma, X. M. Wang, L. C. Tan, Polyoxometalate Metal–Organic Frameworks: Keggin Custers Encapsulated into Silver-triazole Nanocages and Open Frameworks with Supercapacitor Performance. *Inorg. Chem.*, 2019, **58**, 16028-16039.

4 X. J. Yu, S. U. Khan, Z. X. Jin, Q. Wu, H. J. Pang, H. Y. Ma, X. M. Wang, L. C. Tan,
G. X. Yang, Water Cluster Encapsulated Polyoxometalate-based Hydrogen-bonded Supramolecular Frameworks (PHSFs) as a New Family of High-Capacity Electrode Materials. *J. Energy Storage* 2022, **53**, 105192.

5 S. M. Hu, K. Q. Li, X. J. Yu, Z. X. Jin, B. X. Xiao, R. R. Yang, H. J. Pang, H. Y. Ma, X. M. Wang, L. C. Tan, G. X. Yang, Enhancing the Electrochemical Capacitor Performance of Keggin Polyoxometalates by Anchoring Cobalt-Triazole Complexes. *J. Mol. Struct.,* 2022, **1250**, 131753.

6 D. F. Chai, Y. Hou, K. P. O'Halloran, H. J. Pang, H. Y. Ma, G. N. Wang, X. M. Wang, Enhancing Energy Storage via TEA-De-pendent Controlled Syntheses: Two Series of Polyoxometalate-Based Inorganic-Organic Hybrids and their Supercapacitor Properties. *Chem. Electro. Chem.,* 2018, **5**, 3443-3450.

7 G. N. Wang, T. T. Chen, S. B. Li, H. J. Pang, H. Y. Ma, A Coordination Polymer based on Dinuclear (pyrazinyl tetrazolate) copper (ii) Cations and Wells–Dawson Anions for High-performance Supercapacitor Electrodes. *Dalton Trans.,* 2017, **46**, 13897-13902.

8 S. Chinnathambi, M. Ammam, A Molecular Hybrid

Polyoxometalate-Organometallic Moieties and its Relevance to Supercapacitors in Physiological Electrolytes, *J. Power Source* 2015, **284**, 524-535.

9 L. Y. Zhang, S. Di, H. Lin, C. M . Wang, K. Yu, J. H. Lv, C. X. Wang and B.B. Zhou. Nanomaterial with Core–Shell Structure Composed of $\{P_2W_{18}O_{62}\}$ and Cobalt Homobenzotrizoate for Supercapacitors and H_2O_2-Sensing Applications. *Nanomaterials* 2023, **13**, 1176-1192.

10 X. Wang, H. Li, J. F. Lin, C. Y. Wang, X. L. Wang, Capped Keggin Type Polyoxometalate-based Inorganic−organic Hybrids Involving in situ Ligand Transformation as Supercapacitors and Efficient Electrochemical Sensors for Detecting Cr(VI). *Inorg. Chem.,* 2021, **60**, 19287−19296.

11 Y. Hou, D. Chai, B. Li, H. Pang, H. Ma, X. Wang, L. Tan, Polyoxometalate-Incorporated Metallacalixarene@graphene Composite Electrodes for High-Performance Supercapacitors. *ACS Appl. Mater. Interfaces* 2019, **11**, 20845-20853.

12 D. Chai, C. J. Gómez-García, B. Li, H. Pang, H. Ma, X. Wang, Tan, L. Polyoxometalate based Metal-organic Frameworks for Boosting Electrochemical Capacitor Performance. *Chem. Eng. J.,* 2019, **373**, 587-597.